Inhalation Toxicology
International Forum for Respiratory Research

ISSN: (Print) (Online) Journal homepage: https://www.tandfonline.com/loi/iiht20

Pulmonary and systemic toxicity in rats following inhalation exposure of 3-D printer emissions from acrylonitrile butadiene styrene (ABS) filament

Mariana T. Farcas , Walter McKinney , Chaolong Qi , Kyle W. Mandler , Lori Battelli , Sherri A. Friend , Aleksandr B. Stefaniak , Mark Jackson , Marlene Orandle , Ava Winn , Michael Kashon , Ryan F. LeBouf , Kristen A. Russ , Duane R. Hammond , Dru Burns , Anand Ranpara , Treye A. Thomas , Joanna Matheson & Yong Qian

To cite this article: Mariana T. Farcas , Walter McKinney , Chaolong Qi , Kyle W. Mandler , Lori Battelli , Sherri A. Friend , Aleksandr B. Stefaniak , Mark Jackson , Marlene Orandle , Ava Winn , Michael Kashon , Ryan F. LeBouf , Kristen A. Russ , Duane R. Hammond , Dru Burns , Anand Ranpara , Treye A. Thomas , Joanna Matheson & Yong Qian (2020) Pulmonary and systemic toxicity in rats following inhalation exposure of 3-D printer emissions from acrylonitrile butadiene styrene (ABS) filament, Inhalation Toxicology, 32:11-12, 403-418, DOI: 10.1080/08958378.2020.1834034

To link to this article: https://doi.org/10.1080/08958378.2020.1834034

INHALATION TOXICOLOGY
2020, VOL. 32, NOS. 11–12, 403–418
https://doi.org/10.1080/08958378.2020.1834034

Taylor & Francis
Taylor & Francis Group

RESEARCH ARTICLE

Pulmonary and systemic toxicity in rats following inhalation exposure of 3-D printer emissions from acrylonitrile butadiene styrene (ABS) filament

Mariana T. Farcas[a,b], Walter McKinney[a], Chaolong Qi[c], Kyle W. Mandler[a], Lori Battelli[a], Sherri A. Friend[a], Aleksandr B. Stefaniak[a], Mark Jackson[a], Marlene Orandle[a], Ava Winn[a], Michael Kashon[a], Ryan F. LeBouf[a], Kristen A. Russ[a], Duane R. Hammond[c], Dru Burns[a], Anand Ranpara[a], Treye A. Thomas[d], Joanna Matheson[d] and Yong Qian[a]

[a]National Institute for Occupational Safety and Health, Morgantown, WV, USA; [b]Pharmaceutical and Pharmacological Sciences, School of Pharmacy, West Virginia University, Morgantown, WV, USA; [c]National Institute for Occupational Safety and Health, Cincinnati, OH, USA; [d]Office of Hazard Identification and Reduction, U.S. Consumer Product Safety Commission, Rockville, MD, USA

ABSTRACT

Background: Fused filament fabrication 3-D printing with acrylonitrile butadiene styrene (ABS) filament emits ultrafine particulates (UFPs) and volatile organic compounds (VOCs). However, the toxicological implications of the emissions generated during 3-D printing have not been fully elucidated.

Aim and methods: The goal of this study was to investigate the *in vivo* toxicity of ABS-emissions from a commercial desktop 3-D printer. Male Sprague Dawley rats were exposed to a single concentration of ABS-emissions or air for 4 hours/day, 4 days/week for five exposure durations (1, 4, 8, 15, and 30 days). At 24 hours after the last exposure, rats were assessed for pulmonary injury, inflammation, and oxidative stress as well as systemic toxicity.

Results and discussion: 3-D printing generated particulate with average particle mass concentration of $240 \pm 90\ \mu g/m^3$, with an average geometric mean particle mobility diameter of 85 nm (geometric standard deviation = 1.6). The number of macrophages increased significantly at day 15. In bronchoalveolar lavage, IFN-γ and IL-10 were significantly higher at days 1 and 4, with IL-10 levels reaching a peak at day 15 in ABS-exposed rats. Neither pulmonary oxidative stress responses nor histopathological changes of the lungs and nasal passages were found among the treatments. There was an increase in platelets and monocytes in the circulation at day 15. Several serum biomarkers of hepatic and kidney functions were significantly higher at day 1.

Conclusions: At the current experimental conditions applied, it was concluded that the emissions from ABS filament caused minimal transient pulmonary and systemic toxicity.

ARTICLE HISTORY
Received 10 June 2020
Accepted 1 October 2020

KEYWORDS
Thermoplastics; emerging technologies; thermal decomposition; printer emissions; printer emitted nanoparticles; volatile organic compounds; inhalation toxicology; pulmonary toxicity; systemic markers

Introduction

Fused filament fabrication (FFF), a three-dimensional (3-D) printing process, is an emerging technology that has recently gained wide popularity among both consumers and manufacturers due to their increased product efficiency, reduced waste, and greater design flexibility. This makes 3-D printing a valuable tool for more sustainable manufacturing and may represent the next generation of manufacturing processes. The projected global market for 3-D printing and related services is expected to grow to almost 50 billion U.S. dollars by 2025 (www.statista.com), with 6.7 million unit shipments of 3-D printers by 2020. There are many types of 3-D printers used in consumer settings including those that use solid (filments) or liquid matrices. The chemical composition and resulting emissions of these types of printers need further investigation.

FFF 3-D printing involves heating a plastic filament to its melting point and extruding it layer-by-layer to build an object. It has been found that during the thermal decomposition of the filaments, numerous incidental ultrafine particles (UFP) and gaseous or volatile organic compounds (VOCs) with potential adverse respiratory health effects are released into the air (Azimi et al. 2016; Deng et al. 2016; Zhang et al. 2017; Stefaniak et al. 2017a; Davis et al. 2019; Ding et al. 2019; Gu et al. 2019; Stefaniak et al. 2019; Yi et al. 2019). Currently, there are a very limited number of toxicity studies of FFF 3-D printer emissions. In our previous study (Farcas et al. 2019), we evaluated the toxicity of 3-D printing emissions with ABS filaments (referred to as ABS-emissions thereafter) in an *in vitro* model using human small airway epithelial cells (SAEC). We found that the mean particle size of the 3-D emissions in cell culture medium was 202 ± 8 nm, and styrene was the predominant VOC. At 24 hours (h) post-exposure, ABS-emissions caused

CONTACT Yong Qian yaq2@cdc.gov Pathology and Physiology Branch, Health Effects Laboratory Division, National Institute for Occupational Safety and Health, 1095 Willowdale Road, Morgantown, WV 26505, USA

Supplemental data for this article can be accessed at https://doi.org/10.1080/08958378.2020.1834034.

significant dose-dependent cytotoxicity, oxidative stress, apoptosis, necrosis, and production of pro-inflammatory cytokines and chemokines in SAEC cells. Similar findings were reported by another group (Zhang et al. 2019), which showed that particles in ABS-emissions from a consumer-level 3-D printer caused decreased cell viability and increased oxidative stress and inflammatory responses. Stefaniak et al. (2017a) investigated the acute toxic effects of ABS-emissions on cardiovascular function via nose-only inhalation study in rats. Exposure to 1 mg/m^3 ABS-emission for 3 h induced significantly higher mean arterial pressure concomitant with elevated resting arteriolar tone and impaired endothelium-dependent arteriolar dilation. Their results indicated that the 3-D printer emissions could potentially induce systemic toxic effects, similar to what was described previously in relation to inhalation of nanoparticles and ultrafine particulate (UFPs) matter (Nurkiewicz et al. 2004; Rundell et al. 2007; Nurkiewicz et al. 2008). In a health survey, about 60% of participants using 3-D printing in commercial prototyping businesses, educational institutions, and public libraries, reported weekly respiratory symptoms (Chan et al. 2018). The same study also determined that working more than 40 h per week was significantly associated with asthma or allergic rhinitis diagnosis. In a randomized, cross-over design study, healthy human volunteers were exposed to ABS 3-D printer emissions for 1 h (Gumperlein et al. 2018). No acute effects on inflammatory markers in nasal secretions or urine were found. However, a slight increase in exhaled nitric oxide was noted, which could be induced by eosinophilic inflammation from inhaled UFPs. In a case report study (House et al. 2017), a self-employed businessman with a history of childhood asthma operated ten 3-D printers with ABS filaments in a small work area, and, after 10 days working with ABS printing, he experienced chest tightness, shortness of breath, and coughing.

Given that the use of this technology has expanded from workplaces/industry or small businesses to schools and homes and the lack of data addressing the toxicity of emissions, there is a critical need to fill knowledge gaps and assess the potential toxicological effects of exposure to the FFF 3-D emissions, which would help to establish effective control strategies and exposure limits for specific materials to prevent adverse health effects from 3-D printing emission exposure. This study sought to evaluate the *in vivo* respiratory and systemic toxicity of emissions from FFF 3-D printing with ABS filaments. A real-time 3-D printer generation system was designed to allow for simultaneous printing of three commercially available desktop 3-D printers and delivery of an aerosol comprised of a mixture of particles and VOCs to the animal exposure chamber. A time-course exposure study was conducted via whole-body inhalation exposure. Male Sprague-Dawley rats were exposed to a single concentration (240 µg/m^3 ABS average particle mass concentration) for 4 h/day throughout five exposure durations: 1, 4, 8, 15, and 30 days (4 days/week). At 24 h after the last exposure, histopathological changes in the nasal cavity tissue and pulmonary injury, inflammation, and fibrotic responses, as well as systemic toxicity blood markers, were assessed.

Materials and methods

Three-dimensional printer emissions inhalation exposure system

An inhalation exposure system was specifically designed and constructed to deliver FFF 3-D printer emissions to a whole-body rodent exposure chamber (Figure 1). The airtight 55 cm × 55 cm × 50 cm (L × W × H) exposure chamber was constructed out of 16-gauge stainless steel with a clear polycarbonate door. The system automatically controlled chamber pressure, airflow, temperature, particle concentration, and exposure time using custom software. During exposures, rats were housed in a stainless-steel cage rack, which could hold up to 12 rats in individual cage partitions. The cage rack rested on top of cage support beams, which were 1 cm outside diameter stainless steel tubes with small holes (0.33-cm diameter) drilled into the undersides. Each hole was placed at the center of each cage partition such that aerosols would be drawn to each animal's breathing space.

The exposure chamber discharged exhaust air into a carbon/HEPA filter bank. The flow rate of the exhaust was controlled by a mass flow controller (MCRW-50-DS; Alicat Scientific, Tucson AZ) that had its downstream port connected to a vacuum. During exposures, this flow was held constant at 30 l/min. The air entered the top of the exposure chamber either from being pulled through an airtight chamber (50 cm × 64 cm × 122 cm L × W × H) that housed 3 consumer-grade desktop FFF 3-D printers (Manufacturer A) or from a mass flow controller (MCR-50, Alicat Scientific) that provided filtered dilution air.

The exposure chamber pressure was monitored using a differential pressure transducer (Model 264; Setra Systems, Inc. Boxborough MA). Under typical exposure conditions, filtered air was set to zero flow, and the pressure inside the exposure chamber was −6.35 cm H_2O to ambient. This slight negative pressure pulled air from the 3-D printer housing chamber into the exposure chamber via conductive silicone tubing (0.80 cm ID). Room air entering the 3-D printer housing chamber first passed through a HEPA filter and carbon bed.

The temperature and relative humidity inside the exposure chamber were continuously monitored using an electronic probe (HMP60; Vaisala Corporation, Helsinki Finland). The 3-D printers produced significant heat during operation. Therefore, the inhalation exposure chamber was fitted with a cooling device to maintain air temperatures between 22 and 24 °C. This was necessary for animal welfare and was more representative of the real-world exposure condition where room air helps cool down the heat emission in larger spaces. A thermoelectric module (CP-110; TE Technology, Inc., Traverse City, MI) was fitted to the outside back wall of the exposure chamber using four mounting holes. Inside the exposure chamber, custom cooling fins were mounted through the same four mounting holes directly onto the other side of the thermoelectric module.

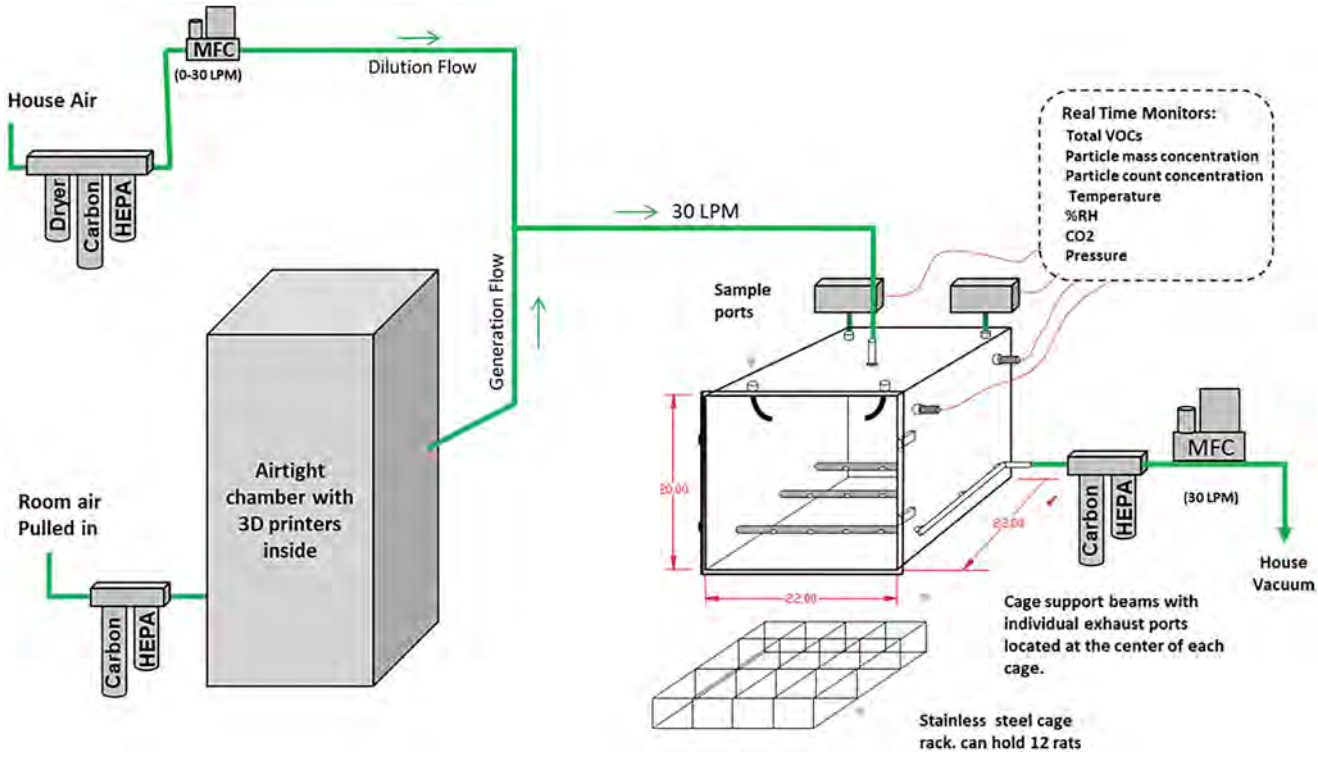

Figure 1. Diagram of the custom-built computer automated inhalation exposure system for testing the ABS 3-D printing emissions. The exposure chamber air was exhausted into a carbon/high-efficiency particulate air (HEPA) filter bank. The flow rate of this air was controlled by a mass flow controller that had its downstream port connected to a hose vacuum. During exposures, this flow was held constant at 30 l/min (LPM). The airflow was controlled using multiple mass flow controllers (MFC) operated at continuous flow rates. Animals were exposed to fumes (particles and gasses) generated from three commercially available 3-D printers placed inside an airtight chamber (300 l volume).

These cooling fins were made of 6061 aluminum and had two circulating fans. The exposure system's custom software monitored the exposure chamber's air temperature and activated the cooler as needed. The two circulating fans always remained active during operation.

Three-dimensional printer settings for ABS filament

The three FFF 3-D printers were each programmed to print simultaneously an object shown in Supplemental Figure S1 from a commercially available ABS filament. The objects printed were 12.7 cm wide by 12.7 cm long, with a height of about 2.54 cm. The width and length were chosen because it occupied most of the build plate. Preliminary testing showed that this type of object produces more particles than a part with a smaller footprint. The object used 240 g of filament to fully print. The 3-D printers all used a nozzle size of 0.4 mm. When not in use, the filament was stored at room temperature in an airtight dry box. Supplemental Table S1 details the 3-D printer settings. These settings produced 3-D printed parts without layer separation, warping, and a smooth outer surface.

ABS emissions collection and characterization

Particle collection and characterization

The aerosol mass concentration inside the exposure chamber was continuously monitored with a Data RAM (DR-40000; Thermo Electron Co., Waltham, MA), and gravimetric determinations (37 mm cassettes with 0.45 µm pore-size Teflon filters, 2 l/min sample flow) were used to calibrate and verify the Data RAM readings during each exposure run. For this study, a 4-h average concentration of 250 µg/m^3 was delivered. Particle counts were also recorded by the custom software connected to a condensation particle counter (CPC) (Model 3787; TSI Inc. Shoreview, MN.).

A fast mobility particle sizer (FMPS, Model 3091, TSI Inc., Shoreview, MN) was used to collect particle size data in 5-s intervals during several 4-h test exposures. The test exposures were conducted in the same manner as a typical exposure run, but without animals present in the exposure chamber. In addition, during these test runs, a field

Table 1. VOCs in the ABS-emissions were sampled and analyzed according to NIOSH Manual of Analytical Methods (NMAM) 3900 (NIOSH 2018).

Compound	Average (ppm)	Standard deviation	OSHA PEL (ppm)	NIOSH REL (ppm)
2,3-Hexanedione	0.0011	0.0022	None	None
Acetaldehyde	0.1105	0.0331	200	None
Acetone	0.0112	0.0109	1000	250
Acetonitrile	0.0045	0.0037	40	20
Benzene	0.0036	0.0014	1	0.1
D-Limonene	0.003	0.0015	None	None
Ethanol	0.019	0.0106	1000	1000
Isopropyl Alcohol	0.0034	0.0067	400	400
Methyl Methacrylate	0.0037	0.003	100	100
Styrene	0.0024	0.003	100	50
Toluene	0.0084	0.0168	200	100
m,p-Xylene	0.0024	0.0005	100	100

emission – scanning electron microscope (FE-SEM; Hitachi S-4800, Tokyo, Japan) was used to analyze particle physical morphology by drawing aerosol samples, for 20 min at a flow rate of 1 l/min, from the exposure chamber onto 25 mm 0.1 µm pore sized polycarbonate filters.

VOCs collection and characterization

VOCs in the ABS-emissions were sampled and analyzed according to NIOSH Manual of Analytical Method (NMAM) 3900 (NIOSH 2018). The emissions were sampled using fused-silica lined, evacuated canisters (450 ml; Entech Instruments Inc., Simi Valley, CA) with a 3-h capillary flow controller and analyzed for a suite of VOCs using an Entech 7200/7650 preconcentration system coupled with an Agilent 7890/5975 gas chromatrograph/mass spectrometer (GC/MS) (Santa Clara, CA). These samples were taken from the exposure chamber during the first 4-h of test runs without animals present. The VOC collection was repeated on five different days, and the average and standard deviation were calculated for each VOC identified.

Animals

Male Sprague-Dawley [Hla: (SD) CVF] (SD) rats (6–7 weeks old, 200–225 g) were purchased from Hilltop Lab Animals (Scottdale, PA), housed in ventilated polycarbonate cages and acclimated for at least seven days before the study began. The animals were provided HEPA-filtered air, irradiated Teklad 2918 diet (Harlan, Madison WI), a combination of ALPHA-dri® and Teklad sani-chips as bedding and tap water ad libitum. Rats were housed four per cage with a 12-h light-dark cycle, and the facility was maintained at 22 ± 2 °C and 40–60% humidity. The study protocol was reviewed and approved by the CDC-Morgantown Institutional Animal Care and Use Committee. The CDC-Morgantown Institutional Animal Care and Use Committee is accreditated by the AAALAC International.

Experimental design

After acclimatization, the animals were randomly divided into two groups (n = 8 per group) and exposed by whole-body inhalation to HEPA- and carbon-filtered air or an average concentration of 240 µg/m^3 ABS-emissions, 4 h/day, 4 days/week for 1, 4, 8, 15, and 30 day exposure durations. (Additional information regarding the animal exposure paradigm can be found in the Supplemental material). At 24 h after the last exposure, the rats were euthanized following an intraperitoneal injection of 100-200 mg sodium pentobarbital/kg body weight (Fort Dodge Animal Health; Fort Dodge, IA). Whole blood was collected from the abdominal aorta and transferred to two collection tubes: a vacutainer containing EDTA (used for whole blood hematological analysis), and a vacutainer containing clot activator and a polymer gel (used for serum chemistry analysis) (Becton-Dickinson; Franklin Lakes, NJ). After clamping the left lung lobe and tying off the right cardiac lobe, bronchoalveolar lavage fluid (BALF) was collected from the remaining right lobes (BALF collection further described below). After lavage, the tied-off right lung lobe and the lavaged right lobes were collected and stored at −80 °C. The left lung lobe and the head/nasal tissues were preserved for histopathological evaluation (Representation of experimental design is displayed in Supplemental Figure S2).

Particle deposition estimates in the nasal passages, tracheobronchial, and alveolar regions

The ABS-emissions particle deposition mass for the head/nose region, tracheobronchial region, alveolar region, and the sum of the tracheobronchial and alveolar regions were estimated using the MPPD model (Anjilvel and Asgharian 1995) based on two different scenarios: without clearance and with clearance, respectively. Furthermore, the *in vivo* alveolar deposition estimates were compared to our previous *in vitro* SAEC study results (Farcas et al. 2019; Supplemental material).

Particle deposition mass without clearance

Particle mass deposition in nasal passages and lung regions was calculated. The size distribution data (particle count based) provided by the FMPS of the ABS-emissions inside the exposure chamber was converted to mass distribution. For this conversion, all particles were assumed spherical with a density of 1.04 g/cm^3 (density of the ABS filament). The FMPS instrument software was used for the calculations. This estimated mass distribution was used as input into the MPPD model (Anjilvel and Asgharian 1995) with the following parameters: animal breathing rate of 120 breaths/min, tidal volume of 1.7 ml, 4-h of total exposure time, and 240 µg/m^3 as the 4-h average concentration.

Particle deposition mass with clearance

Exposures were conducted for four consecutive days, followed by three rest days. In order to account for clearance, deposition in the nose, tracheobronchial and alveolar regions calculated in the model without clearance were used in a discrete-time model that accounted for clearance from each region between the daily exposures. The particle mass deposited for a day of exposure was taken from the one-day exposure particle mass depositions listed in the model without the clearance described above. The deposition for each region was assumed to be the same each subsequent day of exposure. On each day, the amount of material remaining in each region was taken as the sum of the amount present in that region from the previous day, plus the one-day exposure particle mass deposition, minus one-day clearance for each region. The one-day clearance percentages were 100% for the nose, 90% for the tracheobronchial region, and 4% for the alveolar region. This was repeated for the first four-day exposure. For the next three rest days (Friday, Saturday, and Sunday), only clearance from the various compartments was assumed. The process of 4 day exposures and 3 rest days with daily clearance patterns was repeated

for the remaining exposure duration groups (8, 15, and 30 days).

Bronchoalveolar lavage (BAL) analysis

BAL fluid collection and cytology

After exsanguination, the trachea was cannulated, the chest cavity opened, and BALF collected from the right lung (except the cardiac lobe) via the tracheal cannula. The first BAL fraction was obtained by gently filling the right lung with 6 ml cold PBS, massaging for 30 s, withdrawing, and repeating the process for another 30 s. The second BAL fraction consisted of subsequent aliquots of 5 ml PBS (instilled and withdrawn) that were combined until a 15 ml volume was obtained. Both BAL fractions were centrifuged (800 × g for 10 min at 4 °C). The supernatant from the first fraction was set aside to measure total protein, lactate dehydrogenase activity, as well as surfactant and cytokine levels. After discarding the supernatant from the second BAL fraction, the cell pellets from both BAL fractions were combined, resuspended in 1 ml of PBS (Lonza, Pearland, Texas), and aliquots were used to determine the total cell number and cell differential. Briefly, total cell counts were quantified using a Beckman Coulter Multisizer 4 particle counter (Coulter Electronics; Hialeah, FL) and morphology identified using cytospin preparations stained with HEMA solutions (Fisher Scientific; Kalamazoo, MI), counting at least 500 cells per slide. The numbers of alveolar macrophages (AMs), polymorphonuclear leukocytes (PMNs), lymphocytes, and eosinophils were normalized to the total number of cells.

Transmission electron microscopy (TEM) staining of BAL cells

BAL cells were fixated in 1 ml Karnovsky's fixative (2.5% glutaraldehyde, 2.5% paraformaldehyde in 0.1 M sodium cacodylic buffer) and stored at 4 °C until processing. The cells were post-fixed in 2% osmium tetroxide for 1 h, mordanted in 1% tannic acid, and stained *en* bloc in 0.5% uranyl acetate. After a graded series of ethanols for dehydration, the samples were infiltrated in propylene oxide. The samples were embedded in EPON™ (epoxy resin). The blocks were sectioned at 70 nm, and the resulting grids were stained with 4% uranyl acetate and Reynold's lead citrate. The sections were imaged on a JEOL 1400 transmission electron microscope (JEOL, Tokyo, Japan).

Scanning electron microscopy (SEM) images of lungs

A 5-micron non-lavaged lung paraffin section was mounted on a carbon planchet and deparaffinized with propylene oxide for 30 min. The sample was sputter-coated with gold-palladium for 30 s and imaged using a Hitachi S4800 field emission scanning electron microscope (Tokyo, Japan) at 5 KV.

Total protein and LDH activity

Total protein levels and lactate dehydrogenase (LDH) activity were evaluated from the acellular first BAL fraction by using the Pierce™ BCA Protein Assay Kit (Fisher Scientific), and Lactate Dehydrogenase Reagent Set (Pointe Scientific; Lincoln Park, MI), respectively. Data were acquired using Synergy H1 Microplate Reader (BioTek; Winooski, VT).

Surfactant proteins A and D

Surfactant protein A and D, known to contribute to surfactant homeostasis and pulmonary immunity, were quantified from the threefold diluted first BAL fractions using surfactant associated protein A (SP-A) and surfactant associated protein D (SP-D) kits (Biomatik USA, Wilmington, DE), according to the manufacturer guidelines. Data were acquired using Synergy H1 Microplate Reader (BioTek, Winooski, VT).

BALF cytokines levels

The levels of pro- and anti-inflammatory cytokines were measured from undiluted first BAL fraction, i.e. interleukin (IL)-1β, IL-4, IL-5, IL-6, IL-10, IL-13, interferon (IFN)-gamma, neutrophil-activating protein 3 (KC/GRO), and tumor necrosis factor (TNF)-alpha were measured from undiluted first BAL fractions using a V-PLEX Pro-inflammatory Panel 2 Rat Kit (MSD; Meso Scale Discovery, Rockville, MD), according to the manufacturer protocol. Data were acquired using a QuickPlex SQ 120 plate reader (MSD).

Oxidative stress markers

The right lung (except the cardiac lobe) was homogenized with a Bead Mill 24 Homogenizer (Fisher Scientific International, Inc.; Hampton, NH) for 2 min at 4 °C in 1 ml cold PBS (pH 7.4) containing protease inhibitor cocktails and EDTA (Halt™ Protease Inhibitor Cocktails, Thermo Scientific™, Waltham, MA). The protein carbonyl and the malondialdehyde (MDA) levels were quantified from 100-fold diluted lung homogenate suspensions using Protein Carbonyl content and Lipid Peroxidation assay kits (Cell Biolabs, Inc.; San Diego, CA), respectively, according to the manufacturer's protocol. Data were acquired using a Synergy H1 Microplate Reader (BioTek, Winooski, VT). The concentrations were normalized to the total protein content determined using the Pierce™ BCA Protein Assay Kit (Fisher Scientific International, Inc., Hampton, NH).

Blood processing and analysis

Whole blood collected from each rat was equally divided between a vacutainer tube containing EDTA as an anticoagulant (hematological analysis) and a tube containing spray-coated silica, to help in clotting, and a polymer gel (serum separation and analysis).

Characterization of blood cells and hematological parameters

Complete blood count (CBC) tests were performed 30-45 minutes post-exposure to evaluate hematological parameters, which included peripheral erythrocyte and leukocyte counts, leukocyte differentials (percent lymphocytes, neutrophils, monocytes, basophils, and eosinophils), platelet counts, mean platelet volume (MPV), hemoglobin levels, hematocrit, mean corpuscular hemoglobin (MCH) and hemoglobin concentration (MCHC), red blood cell distribution width (RDV), reticulocyte counts, mean platelet volume (MCV), and platelet distribution width (PDW), using a ProCyte Dx Hematology Analyzer (IDEXX Laboratories, Inc., Westbrook, ME).

Serum chemistry profile

For serum chemistry analysis, the whole blood was allowed to clot at room temperature and centrifuged at 2,500 rpm for 10 min. Using a Catalyst One Chemistry Analyzer (IDEXX Laboratories, Inc., Westbrook, ME), the following serum biochemical parameters were evaluated: albumin (ALB), globulin (GLOB), alkaline phosphatase (ALKP), alanine aminotransferase (ALT), aspartate aminotransferase (AST), blood urea nitrogen (BUN), calcium (Ca), cholesterol (CHOL), creatine kinase (CK), creatinine (CREA), C-reactive protein (CRP), lactate dehydrogenase (LDH), ammonia (NH_3), inorganic phosphate (PHOS), total bilirubin (TBIL), total protein (TP), triglycerides (TRI), and uric acid (URIC).

Serum cytokine levels

The levels of pro- and anti-inflammatory cytokines IL-1β, IL-4, IL-5, IL-6, IL-10, IL-13, IFN-gamma, KC/GRO, and TNF-α were determined from samples diluted fourfold using the V-PLEX Pro-inflammatory Panel 2 Rat Kit (MSD), according to the manufacturer protocol. Data were acquired using a QuickPlex SQ 120 plate reader (MSD).

Serum immunoglobulin E (IgE)

The quantity of immunoglobulin E (IgE) was measured from twofold diluted samples using a Rat IgE ELISA Kit (Abcam; Cambridge, MA), according to the manufacturer's protocol. Data were acquired using a Synergy H1 Microplate Reader (BioTek).

Lung and nasal passages histopathological evaluation

The left lung (non-lavaged) was inflated with 10% neutral buffered formalin (NBF), embedded in paraffin, cut at 5 microns on Schott slides, and stained with Hematoxylin and Eosin (H&E) for histopathological evaluation. Lesions were reviewed by a board-certified veterinary pathologist and classified as following: within normal limits (WNL); 1, minimal (change barely exceeds that which is considered normal); 2, mild/slight (the lesion is easily identified but is of limited severity); 3, moderate (the lesion is prominent, but there is significant potential for increased severity); 4, severe (the change is as complete as possible, occupies the majority of the organ).

After the lungs were processed, the nasopharynx was lightly flushed with 10% NBF, and the nasal passages were collected. Nasal tissues were fixed in formalin for approximately one week, then decalcified in 13% formic acid. Standard nasal sections (T1, T2, T3, and T4) were taken (Young 1981). The sections were embedded in paraffin, cut at 5-microns, and stained with H&E.

Statistical analysis

All statistical analyses were performed using SAS/STAT for Windows v9.4. Two-way analyses of variance (treatment by duration) were performed on the measured variables. Post-hoc comparisons between relevant groups were performed using Fishers LSD. All analyses are considered significant at $p < 0.05$.

Results

ABS printing emissions characterization

Particle mass and count concentrations

Chamber particle concentration readings during four representative exposure runs are shown in Figure 2. All runs shown had the same 4-h mass average of 240 μg/m^3. In order to ensure that the same 4-h average particle mass was delivered daily at a constant and repeatable exposure dose, the exposure system software calculated every two sec what the 4-h average mass concentration would be if particles were immediately not delivered to the exposure chamber. If the mass concentration exceeded 240 μg/m^3, the system automatically set the mass flow controller for the dilution flow to 30 l/min, thus providing the exposure chamber with filtered air rather than air from the 3-D printer housing chamber. This method of average particle concentration control was used because significant inconsistencies were observed, day-to-day, in particle generation from the 3-D printers even though they were all ABS printers from a single manufacturer.

The average mass concentration, determined with gravimetric filters, was 240 μg/m^3 with a standard deviation of 90 μg/m^3, and the daily average count concentration measured by the CPC was 88,400 particles/cm^3 with a standard deviation of 23,000 particles/cm^3. Typical particle count concentrations peaked during the first 10 min of printing at about a million particles per cm^3, and from 20 min to 120 min, the count concentration slowly declined. From 120 min to the end of the print job, the particle count gradually increased. Particle mass readings peaked between 40 and 60 min into the print job, then slowly decreased either through the remaining print job or had a second peak mid-print (120 min).

Particle size

A typical size distribution plot (particle count based) of the ABS-emissions inside the exposure chamber during a test run is shown in Figure 2(B). This type of data was collected

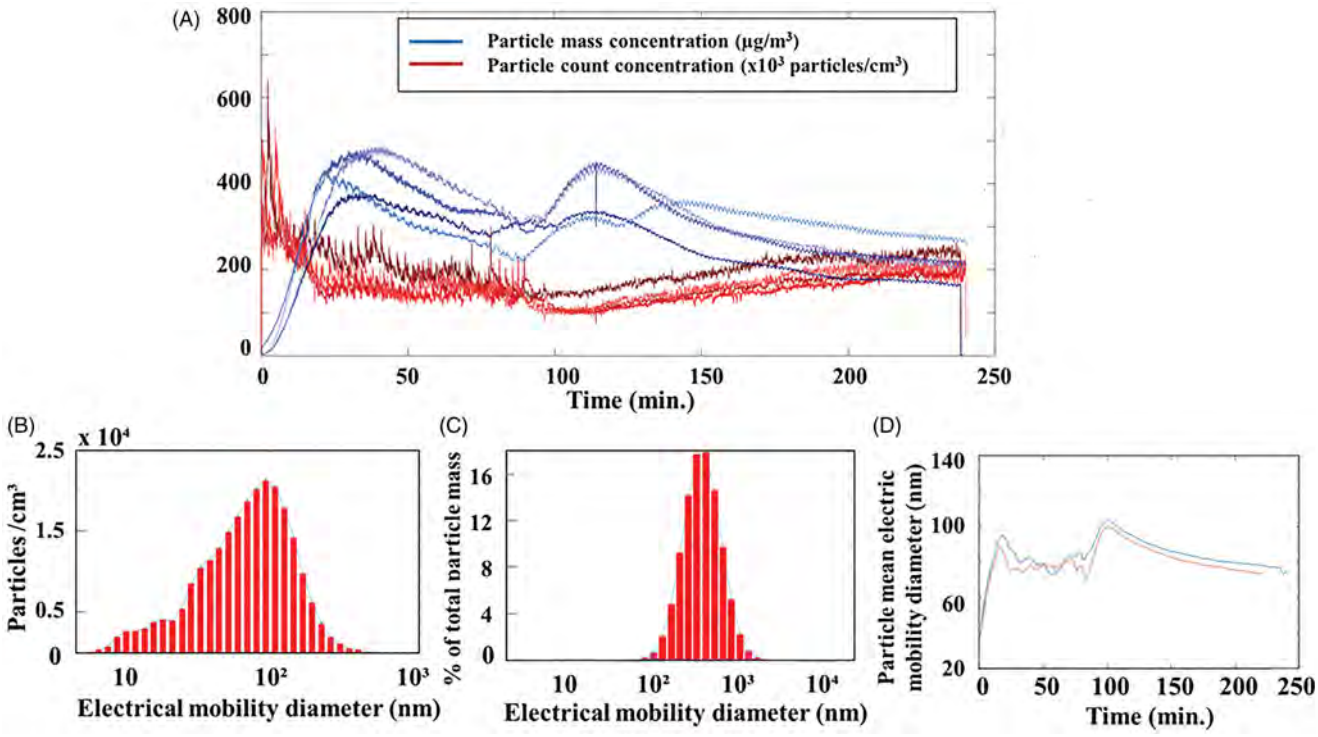

Figure 2. Chamber particle characterization. (A) Particle mass concentrations (red lines), and particle counts (blue lines) over time; (B) particle size distribution plot count-based; (C) particle size distribution from count-based converted to mass by assuming all particles were spherical and had a density of 1 g/cm^3; (D) particle geometric mean electric mobility diameter during two 4-h print jobs.

every 5 s using the FMPS. Figure 2(C) shows the data from Figure 2(B) converted to mass by assuming all particles were spherical and had a density of 1 g/cm^3. The geometric mean diameter (electric-mobility based) for every 5-s sample during two separate 4-h test runs is shown in Figure 2(D). The geometric mean diameter during the start of the print jobs was 40 nm, and it increased to approximately 85 nm after 20 min and remained between 79 nm to 95 nm for the remainder of the 4-h print. The geometric standard deviation was 1.6.

The particles were also sampled onto filters and imaged with a scanning electron microscope (SEM). Several representative particles are shown in Figure 3. The circular dark holes are the pores in the polycarbonate filter. The typical physical diameters of the particles ranged from 40 nm to 500 nm. Some of the particles were elongated and not perfectly spherical with rounded edges.

Analysis of volatile organic compounds by GC/MS

Table 1 lists the most commonly detected volatile compounds (VOCs) in the emissions from five ABS print runs. The emissions were analyzed by GC/MS over a 4-h collection time. Included in Table 1 are the OSHA and NIOSH permissible exposure limits (PEL) and recommended exposure limits (REL) for these VOCs, respectively, for an 8-h work shift. The levels of benzene and acetaldehyde were the highest among the detected compounds, though much lower than the PEL and REL.

Particle deposition estimates in the nasal passages, tracheobronchial, and alveolar regions

Particle deposition mass without clearance

The particle deposition estimates for the nasal passages, the tracheobronchial, and the alveolar regions are provided in Table 2.

Particle deposition mass with clearance

The results for the estimated particle mass burden remaining in each region after the specified number of days of exposure are given in Table 3.

Pulmonary injury and inflammation

Figure 4 represents SEM images of lungs from animals exposed to ABS-emissions, confirming that the ABS particle reached and deposited in the alveolar region as early as after one day of exposure.

To determine the cellular uptake of particles and morphological changes, a TEM analysis of BAL cells was carried out. Figure 5 revealed the pulmonary ABS particle uptake by alveolar macrophages in BAL cells after one and 30 days of exposure (similar outcomes were observed at all durations of exposure). The images showed particle uptake in membrane-lined vacuoles or particle localization in the cytoplasm (arrows). Gross analysis of the morphological appearance of BAL cells indicated no significant differences in cellular morphology.

For the assessment of pulmonary damage, total lung cells, and differentiated cells were counted in the BALF (Figure

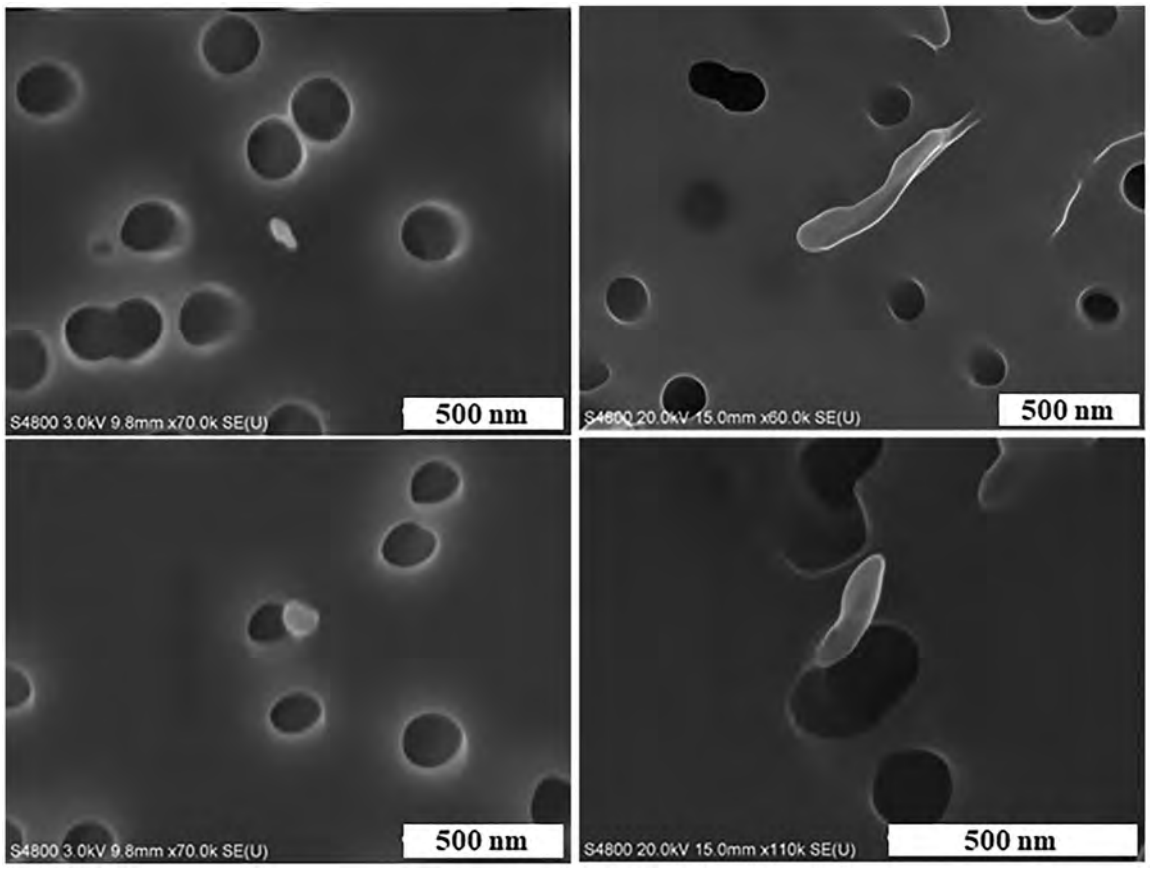

Figure 3. Representative images of ABS 3-D printer-emitted particles indicating surface morphology and elemental composition. 3-D printer emissions were analyzed using FE-SEM. Scale bar at 500 nm for all images.

Table 2. Modeled total lung burden without clearance.

Days of exposure	Particle mass deposited (μg)			
	Nose	Tracheobronchial	Alveolar	Total Lung
1	0.54	0.23	0.85	1.08
4	2.16	0.91	3.41	4.32
8	4.32	1.82	6.81	8.63
15	8.09	3.42	12.77	16.19
30	16.19	6.83	25.54	32.38

Table 3. Modeled lung burden estimates with clearance.

Days of exposure	Particle mass remaining at the end of exposure (μg)			
	Nose	Tracheobronchial	Alveolar	Total Lung
1	0.5	0.2	0.8	1.0
4	0.5	0.3	3.2	3.5
8	0.5	0.3	5.9	6.2
15	0.5	0.3	9.2	9.5
30	0.5	0.3	12.1	12.4

6). The number of macrophages was significantly higher (33%) only at day 15 of exposure. Exposure to ABS emissions caused slightly increased total cell numbers in BALF from day 1 to day 15 of exposure. However, this increase was not significant when compared to air-control rats, and by the 30th day of exposure, total cell numbers returned to control levels. Similarly, there were no significant differences in BALF neutrophil, lymphocyte, and eosinophil counts at any exposure duration, although the numbers of neutrophils and lymphocytes were slightly increased in ABS-exposed rats throughout the entire study.

To further examine pulmonary injury, LDH activity, total protein, SP-A, and SP-D levels in BALF were measured. We found that the LDH activity and total protein levels were not significantly different between the ABS-exposed animals and air-control group at any time point (Figure 7). There were also no significant differences in SP-A and SP-D in the BALF (Figure 8). However, the levels of these two proteins, known for their protective role in lung disease, were slightly decreased in ABS-exposed rats, which suggests that the emissions might have the potential to alter the host's lung immune responses. Specifically, SP-A levels decreased beginning at the 8th day of exposure and persisted until day 30; SP-D levels decreased starting with the 4th day of exposure and lasted until the 15th day of exposure.

To evaluate ABS emission-induced inflammatory responses in airways, a panel of 9 pro- and anti-inflammatory cytokines were measured in BALF. Significant changes were observed in BALF IFN-γ and IL-10 levels, with no significant differences in levels of IL-1β, IL-4, IL-5, IL-6, KC, and TNF-α when compared to air-control rats (Table 4). IFN-γ levels increased early (73% at day 1) and returned to control levels after day 4. Similarly, IL-10 levels significantly increased early, but remained elevated, peaking at day 15 day, a 39% increase compared to air-control animals.

Along with inflammation, oxidative stress is a key mechanism linking particle exposure to observable physiological and biochemical responses. As such, protein carbonyl and MDA levels were measured to determine the extent of

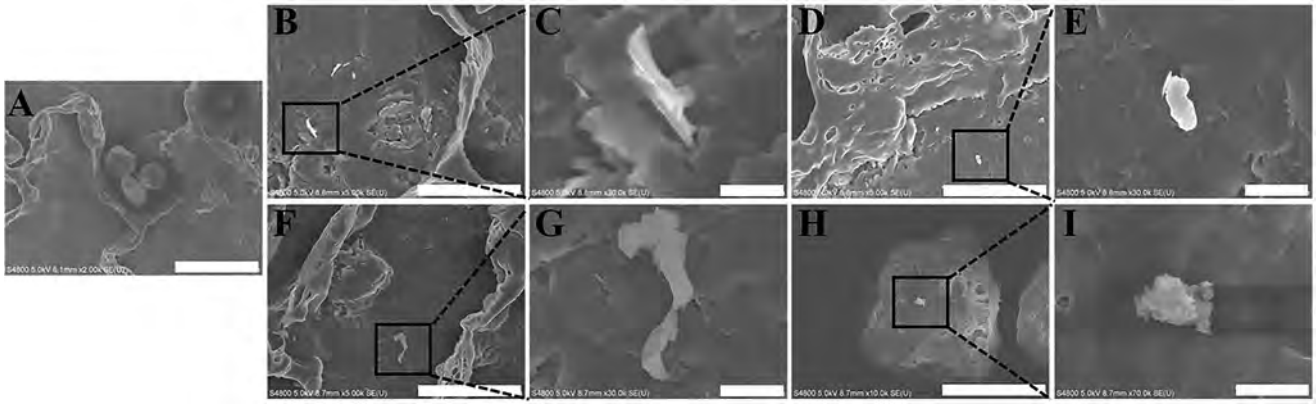

Figure 4. Representative images of ABS particles deposited in the alveolar region at days 1 and 30 of exposure using FE-SEM: (A) air-control, (B, C, D, E) day 1 of exposure, (F, G, H, I) day 30 of exposure. Scale bar at 10 μm for images B, D, and F, 5 μm for image H, 1 μm for images C, E, and G, and 500 nm for image I.

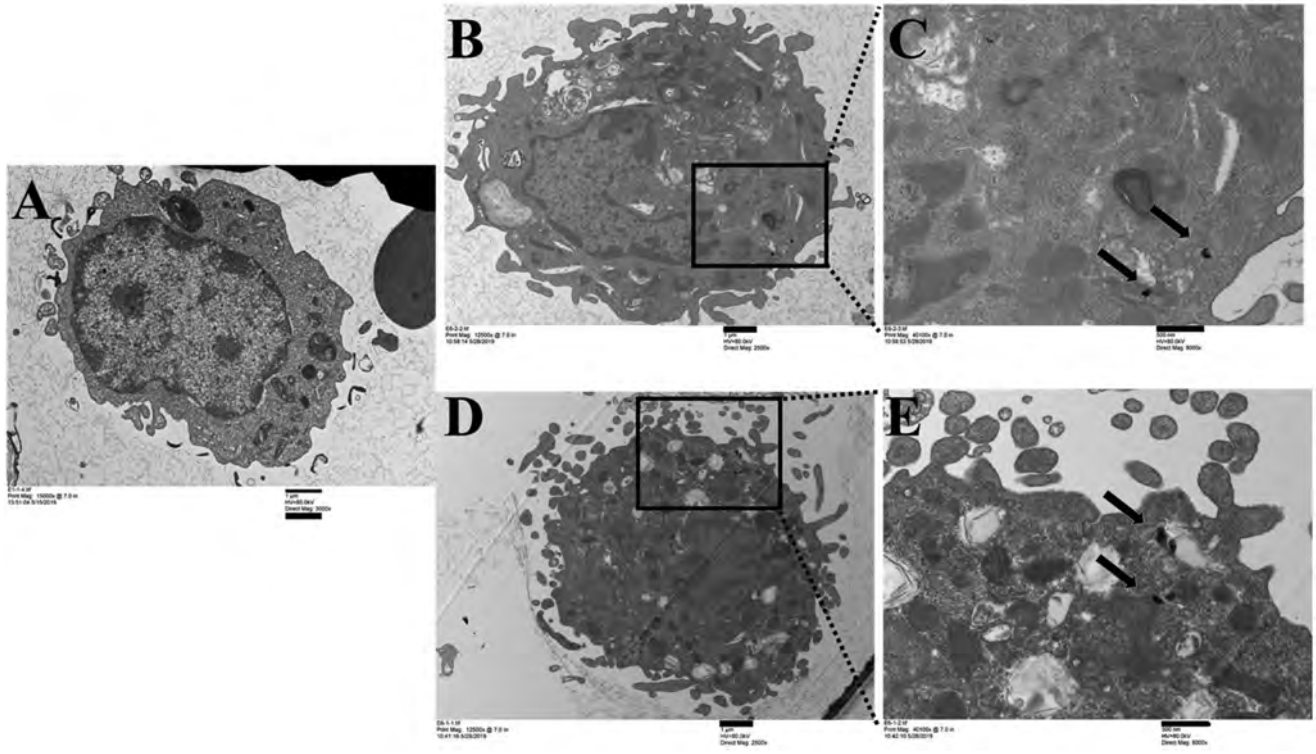

Figure 5. Cellular uptake of ABS particles in BAL cells at days 1 and 30 of exposure by TEM: (A) air-control, (B, C) day 1 of exposure, (D, E) day 30 of exposure. Scale bar at 1 μm for images A, B, and D, and 500 nm for images C and E.

protein and lipid oxidation after exposure to ABS emissions (Figure 9). There were no significant differences in protein carbonyl and MDA levels between exposed and air-control rats at any exposure time point. However, similar to surfactant protein levels, protein carbonyl concentrations were slightly increased in ABS-exposed rats from day 1 through day 15, returning to control values by day 30.

Systemic effects

To assess for exposure-induced systemic toxic effects after pulmonary exposure to ABS emissions, blood samples were analyzed for clinical and hematological parameters, in addition to biomarkers of muscle, metabolic, renal, and hepatic function. Significant increases in platelet (twofold) and monocyte (73%) levels were measured at day 15 of exposure (Table 5), accompanied by a nonsignificant increase in platelet and monocyte populations on day 30 (62% and 39%, respectively) when compared to air-control. There were no significant differences in the other hematological measurements at any time point, although elevations were observed for neutrophils and eosinophils (35% and 53%, respectively), peaking on day 15. Serum chemistry analysis indicates that creatinine kinase and aspartate aminotransferase, markers of hepatic and kidney function, were significantly higher after one day of exposure, returning to control levels by day 4

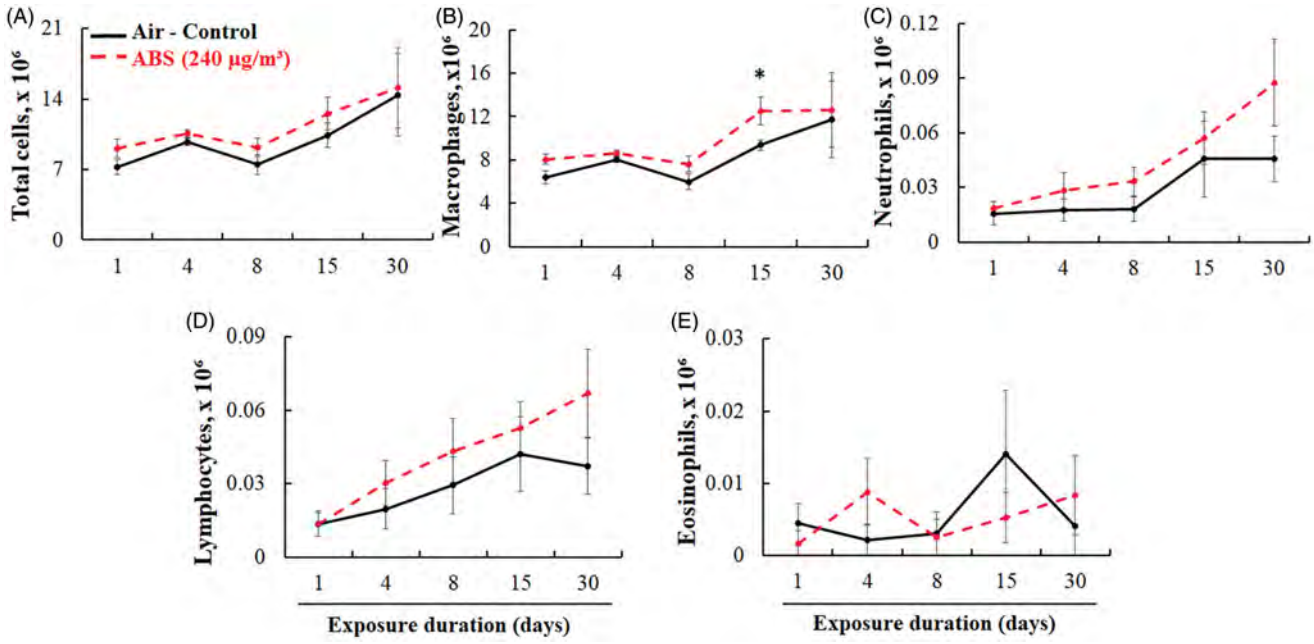

Figure 6. BAL cell differential. Total cells (A), AMs (B), PMNs (C), lymphocytes (D), and eosinophils (E). The rats were exposed for 1, 4, 8, 15, and 30 days to air or ABS emissions (240 µg/m^3) and euthanized at 24 h post last exposure. Values represents means ± SEMs; N = 8/group/time point. *Significantly different from corresponding air control, $p < 0.05$.

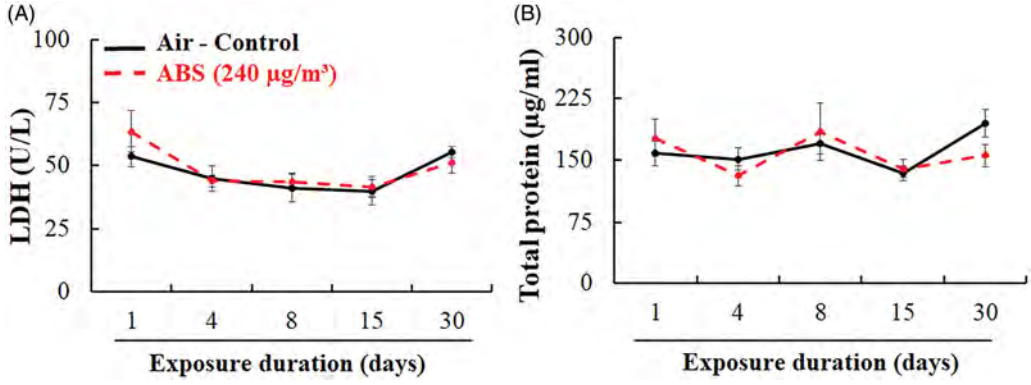

Figure 7. Pulmonary injury markers: LDH activity (A) and total protein (B) in BALF. The rats were exposed for 1, 4, 8, 15, and 30 days to air or ABS emissions (240 µg/m^3) and euthanized at 24 h post last exposure. Values represents means ± SEMs; N = 8/group/time point.

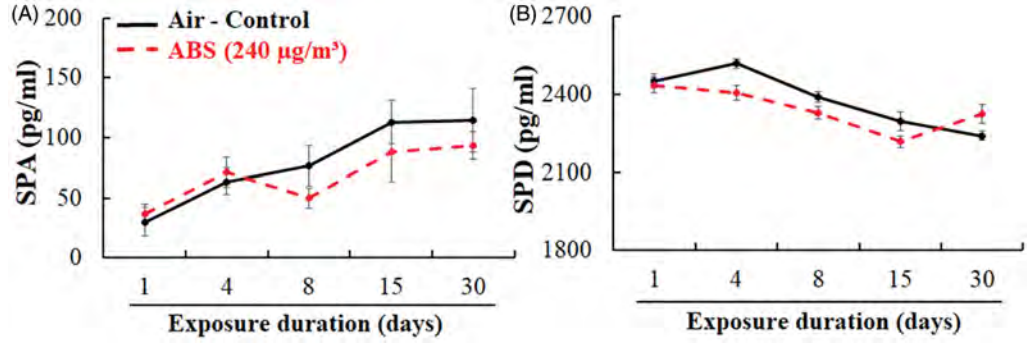

Figure 8. Markers of injury to the alveolar epithelium: surfactant proteins SP-A (A) and SP-D (B). The rats were exposed for 1, 4, 8, 15, and 30-days to air or ABS emissions (240 µg/m^3) and euthanized at 24 h post last exposure. Values represents means ± SEMs; N = 8/group/time point.

(Table 6). In addition, although the levels of inorganic phosphate, and lactate dehydrogenase, markers of hepatic function were within normal intervals, they were significantly higher in ABS-exposed animals when compared to air-controls. Similarly, after 15 days of exposure, blood urea nitrogen, inorganic phosphate, and uric acid were significantly higher, with concentrations falling within standard ranges. No significant changes in any of the serum chemistry markers were observed after 30 days of exposure.

Table 4. Level of cytokines in bronchoalveolar lavage fluid.

		Exposure duration (days)				
Marker	Treatment	1	4	8	15	30
IFN-γ (pg/ml)	Air	1.79 ± 0.34	1.69 ± 0.15	1.62 ± 0.20	1.78 ± 0.15	1.59 ± 0.11
	ABS	3.11 ± 0.62*	2.61 ± 0.48*	2.18 ± 0.20	2.35 ± 0.09	2.13 ± 0.19
IL-10 (pg/ml)	Air	1.79 ± 0.25	2.05 ± 0.18	2.24 ± 0.16	2.14 ± 0.12	2.25 ± 0.11
	ABS	2.37 ± 0.13*	2.53 ± 0.21*	2.57 ± 0.12	2.99 ± 0.10*	2.54 ± 0.15
IL-1β (pg/ml)	Air	4.69 ± 0.30	6.04 ± 1.09	6.40 ± 1.14	5.95 ± 0.57	5.28 ± 0.39
	ABS	4.78 ± 0.42	5.58 ± 0.65	6.60 ± 0.88	6.29 ± 0.35	5.76 ± 0.38
IL-4 (pg/ml)	Air	0.43 ± 0.06	0.47 ± 0.05	0.46 ± 0.03	0.43 ± 0.05	0.51 ± 0.04
	ABS	0.37 ± 0.03	0.43 ± 0.06	0.44 ± 0.04	0.53 ± 0.02	0.48 ± 0.05
IL-5 (pg/ml)	Air	5.98 ± 0.68	6.64 ± 0.93	6.62 ± 0.72	6.46 ± 0.71	6.49 ± 0.45
	ABS	6.01 ± 0.32	6.73 ± 0.57	7.03 ± 0.27	7.72 ± 0.44	7.65 ± 0.58
IL-6 (pg/ml)	Air	80.67 ± 8.91	102.00 ± 7.17	93.59 ± 7.08	111.58 ± 8.93	104.58 ± 8.64
	ABS	91.11 ± 4.73	104.56 ± 11	99.90 ± 3.18	104.62 ± 5.38	105.68 ± 8.56
KC (pg/ml)	Air	89.23 ± 15.6	114.62 ± 25	107.37 ± 15.34	140.42 ± 24.97	141.61 ± 28.79
	ABS	64.82 ± 6.05	80.75 ± 4.53	134.49 ± 24.14	127.99 ± 8.57	113.25 ± 7.84
TNF-α (pg/ml)	Air	1.57 ± 0.17	1.74 ± 0.48	1.95 ± 0.34	1.94 ± 0.29	1.54 ± 0.17
	ABS	2.02 ± 0.21	1.40 ± 0.10	1.80 ± 0.32	1.63 ± 0.21	1.40 ± 0.13

Values represents means ± SEMs; n = 8/group/time point. *$p < 0.05$ versus air-control group.

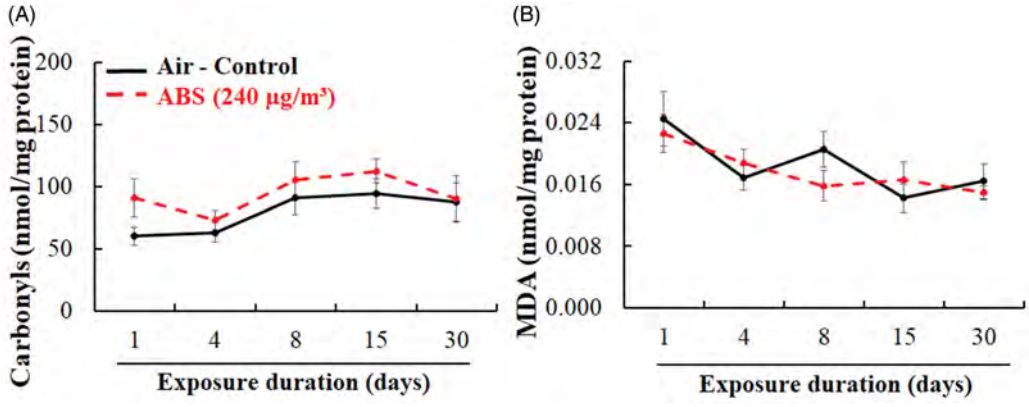

Figure 9. Lung oxidative stress markers: protein carbonyls (A) and malondialdehyde (B). The rats were exposed for 1, 4, 8, 15, and 30 days to air or ABS emissions (240 µg/m^3) and euthanized at 24 h post last exposure. Values represents means ± SEMs; N = 8/group/time point.

The systemic inflammation was further assessed by measuring the response of pro- and anti-inflammatory cytokines (similar panel as assessed in BALF) in serum. Furthermore, there were no significant differences in serum levels of pro- or anti-inflammatory cytokines, at any time point (Supplemental Table S2). Slightly higher serum levels of IFN-γ, IL-6, IL-10, and KC were observed at day 15. IFN-γ, IL-6, and IL-10 remained slightly increased at exposure day 30, as well as serum levels of IL-1β.

No significant difference in serum IgE levels, an immune-mediated marker of allergic response, was observed (Supplemental Figure S4).

Histopathology of lung and nasal passages

H&E stained sections of the left lung lobe and four levels of nasal passages (T1, T2, T3, and T4) were examined for routine histopathology using light microscopy (Olympus BX53). Tissue sections from air-exposed control animals were also examined for determining background pathology. Exposure-related changes were not observed in any lung or nasal passage sections examined, for any treatment group.

Discussion

From industrial, educational to medical and healthcare applications, 3-D printing proves to be an exciting and promising technology (Ahn et al. 2016; Trenfield et al. 2019; Yi et al. 2019; Wang et al. 2020). However, as with any emerging technology, little is known about the toxicity of the emissions generated during printing and how emissions may differ from various types of raw material.

In our study, the ABS-emissions generated during real-time printing with a consumer-grade level 3-D printer included incidental UFPs and VOCs. The temporal pattern and size distributions (including peak, average number, and mass concentrations) of particle emissions were characterized during animal exposures to compare to real-world exposure settings. Particle number concentration in the exposure chamber followed a temporal pattern that consisted of a rapid rise during the first few min of printing, followed by a slower decline throughout the remainder of the print time. A similar pattern was reported for indoor environments (Stephens et al. 2013; Simon et al. 2018) and industrial workplaces (Stefaniak et al. 2019) where FFF 3-D sprinters extrude ABS filament. During animal exposures, peak particle concentrations were about 10^6 particles/cm^3, which is a factor of 15 to 25 higher than levels observed in

Table 5. Hematological parameters.

		Exposure duration (days)				
Parameter	Treatment	1	4	8	15	30
Erythrocytes (M/μL)	Air	4.86 ± 0.58	6.64 ± 0.23	7.27 ± 0.17	7.25 ± 0.50	7.07 ± 0.42
	ABS	5.15 ± 0.42	6.76 ± 0.15	6.90 ± 0.30	7.43 ± 0.32	7.01 ± 0.97
Hemoglobin (g/dL)	Air	10.05 ± 1.20	13.06 ± 0.39	13.79 ± 0.18	13.15 ± 0.86	12.09 ± 0.68
	ABS	10.54 ± 0.80	13.18 ± 0.18	12.91 ± 0.56	13.58 ± 0.54	12.05 ± 1.68
Hematocrit	Air	32.23 ± 2.27	38.57 ± 1.22	40.40 ± 0.94	37.61 ± 2.74	34.93 ± 2.27
(%)	ABS	30.43 ± 2.63	39.11 ± 0.43	37.84 ± 1.88	39.33 ± 1.87	34.95 ± 4.86
MCV	Air	59.64 ± 0.85	58.19 ± 0.66	55.64 ± 0.53	51.75 ± 0.37	49.31 ± 0.39
(fL)	ABS	59.00 ± 0.77	57.96 ± 0.85	54.79 ± 0.54	53.00 ± 0.47	49.13 ± 0.92
MCH	Air	20.71 ± 0.24	19.70 ± 0.18	19.01 ± 0.25	18.18 ± 0.11	17.14 ± 0.12
(pg)	ABS	20.47 ± 0.16	19.54 ± 0.29	18.71 ± 0.16	18.30 ± 0.12	16.68 ± 0.55
MCHC	Air	34.76 ± 0.38	33.87 ± 0.21	34.20 ± 0.43	35.16 ± 0.38	34.75 ± 0.34
(g/dL)	ABS	34.70 ± 0.39	33.70 ± 0.29	34.24 ± 0.29	34.54 ± 0.39	33.94 ± 0.57
RDW-CV	Air	14.71 ± 0.17	14.99 ± 0.31	16.14 ± 0.47	16.78 ± 0.74	19.49 ± 0.88
(%)	ABS	14.42 ± 0.31	15.55 ± 0.56	15.93 ± 0.38	17.71 ± 0.60	20.10 ± 0.78
Reticulocytes (K/uL)	Air	323.79 ± 19	304.61 ± 14	222.24 ± 15	197.94 ± 14	201.98 ± 12
	ABS	311.38 ± 33	324.55 ± 13	215.20 ± 11	221.35 ± 10	243.14 ± 10
Reticulocytes	Air	6.06 ± 0.19	4.60 ± 0.19	3.08 ± 0.24	2.73 ± 0.05	2.86 ± 0.08
(%)	ABS	5.74 ± 0.23	4.82 ± 0.25	3.21 ± 0.32	2.96 ± 0.04	3.05 ± 0.14
Platelets	Air	566.67 ± 56	765.80 ± 53	643.43 ± 158	438.20 ± 167	415.50 ± 109
(K/μL)	ABS	415.67 ± 102	700.20 ± 98	592.17 ± 137	838.67 ± 83*	675.80 ± 89
PDW	Air	8.30 ± 0.27	8.28 ± 0.06	8.36 ± 0.25	8.44 ± 0.45	8.47 ± 0.12
(fL)	ABS	8.00 ± 0.60	8.43 ± 0.22	8.78 ± 0.34	7.95 ± 0.16	8.39 ± 0.14
MPV	Air	7.00 ± 0.17	7.30 ± 0.05	7.16 ± 0.17	7.22 ± 0.25	7.07 ± 0.07
(fL)	ABS	6.75 ± 0.65	7.28 ± 0.08	7.42 ± 0.20	6.83 ± 0.11	7.05 ± 0.16
Leukocytes (K/μL)	Air	4.26 ± 0.72	5.01 ± 0.64	4.41 ± 0.66	4.31 ± 0.57	3.75 ± 0.64
	ABS	2.44 ± 0.65	5.71 ± 0.76	4.59 ± 0.48	4.46 ± 0.47	3.93 ± 0.64
% Neutrophils	Air	6.08 ± 1.12	8.79 ± 1.72	9.82 ± 0.90	8.80 ± 0.73	13.11 ± 1.31
	ABS	4.77 ± 0.87	8.59 ± 0.82	9.78 ± 1.72	11.85 ± 1.18	15.84 ± 1.86
% Lymphocytes	Air	89.34 ± 1.59	87.17 ± 2.47	84.86 ± 1.56	87.13 ± 0.88	80.24 ± 2.98
	ABS	92.58 ± 1.32	86.45 ± 1.32	85.15 ± 2.51	80.56 ± 2.51	77.38 ± 2.23
% Monocytes	Air	2.42 ± 0.22	2.37 ± 0.65	2.50 ± 0.57	2.20 ± 0.28	1.56 ± 0.16
	ABS	1.65 ± 0.19	2.21 ± 0.25	1.85 ± 0.40	3.80 ± 0.51*	2.18 ± 0.38
% Eosinophils	Air	1.24 ± 0.27	1.56 ± 0.54	3.05 ± 0.90	1.71 ± 0.19	5.66 ± 1.92
	ABS	1.16 ± 0.37	1.60 ± 0.28	3.04 ± 0.97	2.60 ± 0.76	4.35 ± 0.87
% Basophils	Air	0.30 ± 0.03	0.27 ± 0.07	0.28 ± 0.06	0.16 ± 0.07	0.38 ± 0.07
	ABS	0.18 ± 0.02	0.27 ± 0.04	0.25 ± 0.03	0.23 ± 0.02	0.35 ± 0.06

Values represents means ± SEMs; n = 8/group/time point. *$p < 0.05$ versus air-control group.

industrial workplaces where FFF 3-D printers extrude ABS filament (Stefaniak et al. 2019). The daily average particle number concentration during animal exposures was 88,000 ± 23,000 particles/cm^3. This daily average value is similar to that reported for a poorly ventilated college dormitory (McDonnell et al. 2016) and a Finnish workplace (Vaisanen et al. 2019), but a factor of three to five higher than reported for other industrial workplaces (Stefaniak et al. 2019). Geometric mean particle diameter was about 40 nm at the start of printing and increased to 80 nm as printing progressed. Although data on aerosol size distribution in occupational environments are sparse, our observed size is similar to that reported for a non-industrial indoor environment (Stephens et al. 2013). Given their small size, UFPs from FFF 3-D printers have a low mass. Vaisanen et al. (2019) measured, via a real-time monitor, a particle mass concentration of 10 μg/m^3 in a workplace. McDonnell et al. (2016), also using a real-time monitor, calculated particle mass concentrations ranging from 120 to 620 μg/m^3 for a dormitory room and small office on a college campus.

Our previous *in vitro* study (Farcas et al. 2019) delivered an average particle concentration of 1×10^7 ABS particles per ml, which would result in an equivalent alveolar lung burden of ABS particles of 758 μg in the rat. In our current study, the day 30 alveolar deposition estimates were 25.54 μg and 12.10 μg, representing the model without and with clearance, respectively, which is about 30 to 60 times lower than the *in vitro* study. As such, we attribute the minimal respiratory and systemic changes observed in this study to lower particle deposition than that delivered in the *in vitro* study.

In terms of VOCs concentrations, we found that all detected VOCs emitted over 4-h print jobs were at average levels that were much lower than workplace exposure limits (REL or PEL), whose values are appropriate for comparison to exposure measurements collected in occupational settings and would not be protective of sensitive individuals or children in non-occupational settings. We identified, styrene, benzene, and acetaldehyde vapor, which may irritate the mucous membranes of the respiratory tract (Nielsen and Alarie 1982; Sittig 1985; EPA/600/8-86-015A 1987). An important finding from previous studies is that filament factors such as the formulation, the temperature to which it is heated, and the brand influences its breakdown and resultant released gas profile (Zhang et al. 2017; Stefaniak et al. 2017b; Davis et al. 2019; Potter et al. 2019). Wojtyła et al. (2017) identified more than 70 different VOCs in ABS filament emissions, with styrene, ethylbenzene, benzaldehyde, formaldehyde, acetophenone, and vinyl cyclohexene as the most abundant. In another study (Kim et al. 2015), found that printing with ABS filaments released ethylbenzene at levels 16.4 times higher than outdoor air concentrations,

Table 6. Serum chemistry profiles.

Marker	Treatment	Exposure duration (days) 1	4	8	15	30	Standard ranges
CREA (mg/dL)	Air	0.13 ± 0.02	0.18 ± 0.02	0.20 ± 0.03	0.21 ± 0.01	0.24 ± 0.02	0.1 – 0.7
	ABS	0.10 ± 0.01	0.16 ± 0.02	0.19 ± 0.02	0.19 ± 0.01	0.21 ± 0.02	
BUN (mg/dL)	Air	15.57 ± 0.65	15.88 ± 0.81	16.63 ± 0.50	14.75 ± 0.96	18.75 ± 0.65	9 – 21
	ABS	15.50 ± 1.29	13.88 ± 0.93	18.63 ± 1.09	17.88 ± 0.93*	19.00 ± 0.60	
PHOS (mg/dL)	Air	9.89 ± 0.31	8.68 ± 0.13	8.41 ± 0.41	7.98 ± 0.21	7.01 ± 0.20	5.8 – 11.2
	ABS	10.93 ± 0.49*	9.26 ± 0.23	9.05 ± 0.26	9.51 ± 0.51*	7.03 ± 0.13	
TP	Air	5.24 ± 0.16	5.25 ± 0.05	5.23 ± 0.10	5.38 ± 0.06	5.51 ± 0.110	5.3 – 6.9
(g/dL)	ABS	5.37 ± 0.10	5.28 ± 0.07	5.24 ± 0.12	5.48 ± 0.14	5.66 ± 0.10	
ALB	Air	2.80 ± 0.15	2.71 ± 0.04	2.73 ± 0.08	2.74 ± 0.05	2.66 ± 0.05	3.8 – 4.8
(g/dL)	ABS	2.85 ± 0.07	2.74 ± 0.05	2.68 ± 0.08	2.86 ± 0.09	2.78 ± 0.05	
GLOB	Air	2.44 ± 0.02	2.54 ± 0.04	2.50 ± 0.05	2.64 ± 0.05	2.85 ± 0.06	1.5 – 2.8
(g/dL)	ABS	2.52 ± 0.03	2.54 ± 0.05	2.56 ± 0.50	2.61 ± 0.07	2.89 ± 0.06	
ALT	Air	63.57 ± 11.12	55.50 ± 5.05	59.38 ± 6.07	51.63 ± 3.35	54.13 ± 4.23	20 – 61
(U/L)	ABS	64.33 ± 5.41	50.25 ± 3.50	61.88 ± 10.95	47.70 ± 7.23	52.50 ± 2.32	
ALKP	Air	215.86 ± 15	227.25 ± 9	186.88 ± 12	184.13 ± 11	161.25 ± 6	16 – 302
(U/L)	ABS	215.17 ± 18	244.38 ± 18	212.38 ± 17	215.17 ± 18	161.25 ± 8	
TBIL (mg/dL)	Air	0.31 ± 0.14	0.14 ± 0.03	0.13 ± 0.03	0.15 ± 0.04	0.13 ± 0.02	0.1 – 0.7
	ABS	0.52 ± 0.11	0.15 ± 0.04	0.15 ± 0.05	0.20 ± 0.08	0.17 ± 0.05	
CHOL (mg/dL)	Air	50.29 ± 3.00	47.250 ± 1.26	39.38 ± 3.54	43.00 ± 3.99	42.50 ± 4.42	20 – 92
	ABS	50.00 ± 3.00	49.57 ± 1.66	36.25 ± 4.86	46.88 ± 2.17	34.75 ± 2.63	
CK	Air	200.80 ± 65	92.00 ± 7	102.50 ± 21	105.70 ± 12	87.45 ± 7	48 – 340
(U/L)	ABS	457.37 ± 64*	120.80 ± 16	118.53 ± 14	108.53 ± 19	99.40 ± 14	
LDH	Air	326.55 ± 45	388.04 ± 56	322.51 ± 90	558.25 ± 66	335.49 ± 42	167 – 1428
(U/L)	ABS	649.80 ± 97*	448.03 ± 76	383.01 ± 65	694.00 ± 25	382.39 ± 34	
URIC (mg/dL)	Air	1.64 ± 0.67	0.68 ± 0.07	1.33 ± 0.87	0.50 ± 0.08	0.45 ± 0.05	0.8 – 4.4
	ABS	1.62 ± 0.43	0.93 ± 0.23	0.80 ± 0.16	1.60 ± 0.59*	0.69 ± 0.08	
AST	Air	128.00 ± 29	100.25 ± 9	106.00 ± 14	108.25 ± 9	87.38 ± 2	39 – 111
(U/L)	ABS	206.00 ± 47*	97.50 ± 8	118.75 ± 19	113.71 ± 13	93.25 ± 7	
NH3 (μmol/L)	Air	57.71 ± 16.95	31.00 ± 7.04	27.75 ± 4.02	25.88 ± 3.76	19.00 ± 3.13	na
	ABS	66.33 ± 14.01	46.13 ± 10.19	34.63 ± 5.23	30.43 ± 5.71	24.50 ± 3.07	
CRP (mg/dL)	Air	0.17 ± 0.02	0.16 ± 0.02	0.19 ± 0.02	0.20 ± 0.05	0.19 ± 0.03	na
	ABS	0.18 ± 0.03	0.16 ± 0.03	0.18 ± 0.03	0.16 ± 0.03	0.16 ± 0.04	

Values represents means ± SEMs; n = 8/group/time point. *$p < 0.05$ versus air-control group.

isovaleraldehyde 11.9 times higher, and acetaldehyde 3.2 times higher. More recently, Davis et al. (2019) detected 177 individual VOCs during FFF 3-D printing with ABS. These studies substantiate the potential for human exposure and subsequent health effects from VOCs emitted during printing. Technologies to reduce and prevent VOC emissions from FFF 3-D printing are emerging. When testing the efficiency of commercially available filter covers and air-purifiers, varying capabilities of these control measures in removing VOCs were observed (Gu J et al. 2019). It was found that conditioning the new filters and pre-operating the control devices for a few days helped to reduce the VOCs emissions. However, these control measures were unable to eliminate VOCs completely, and even produced new types of VOCs, demonstrating that the development of effective control strategies for reducing VOC emissions could be more problematic. Recently, an advanced filtration system such as photocatalytic filtration has been created. It was based on doped graphitic carbon nitride materials and was able to successfully decompose and therefore reduce the emission of hazardous VOCs (Wojtyła et al. 2020).

As noted in our study and previously reported by others (Kim et al. 2015; Azimi et al. 2016; Vaisanen et al. 2019), most incidental particles emitted from FFF 3-D printing are smaller than 100 nm. They, therefore, have the potential to penetrate deeper into the lungs than larger particles and to trigger local inflammatory and oxidative stress effects by activating resident macrophages and epithelial cells (Oberdorster et al. 2005). To evaluate the pulmonary effects of FFF ABS-emissions, we measured inflammatory and injury markers in BALF (cell differential, total protein, LDH activity, surfactant proteins A and D, and pro- and anti-inflammatory cytokines and chemokines) and in lung homogenates (the lipid peroxidation-derived malondialdehyde and protein carbonyl). Furthermore, sections of the left lung lobe and four levels of nasal passages were examined for histopathological changes. We found that after one day of exposure to ABS-emissions, the levels of IFN-γ, one of the most potent macrophage activators (Arango Duque and Descoteaux 2014), spiked significantly in BALF and decreased thereafter. At day one of exposure, we also noted a slight increase in TNF-α, a cell-signaling cytokine produced by activated macrophages and involved in acute systemic inflammation, and IL-6, a cytokine that has both pro-inflammatory and anti-inflammatory functions (Arango Duque and Descoteaux 2014). However, the number of alveolar macrophages in BALF did not increase significantly until the 15th day of exposure, when we also found that a decrease in IFN-γ levels correlated with increased secretion of the anti-inflammatory cytokine IL-10. We speculate that at earlier time points, the macrophages were activated by the pro-inflammatory mediators IFN-γ and TNF-α released in response to subtle injuries, resulting in the macrophages adhere to the alveolar lung wall, as previously reported (Castranova et al. 1987; Mandler et al. 2019). To counteract the tissue-damaging potential of the pro-inflammatory state of 'classically activated' (Mosser 2003) macrophages (M1 phenotype), a switch to an anti-inflammatory or reparative

state, 'alternatively activated' or M2 phenotype (Koh and DiPietro 2011), occurred stimulated by the production of anti-inflammatory markers, such as IL-10.

This injury-repair response may explain the 'delayed' influx of alveolar macrophages at the damaged site and its peak occurrence in BALF at the 15th day of exposure, which corresponded with increased blood monocytes and platelets. These results tie to previous studies (Fujii et al. 2002; Goto et al. 2004) that demonstrate that inflammatory signals (e.g. cytokines) produced by alveolar macrophages after phagocytosis of particles can stimulate the release of monocytes from the bone marrow into the circulation. Monocytes that are attracted to the injured site by growth factors released by platelets enter the lung through blood vessel walls and mature into macrophages (Lorenz and Longaker 2008). Increased platelet count is a notable finding as it is also associated with cardiovascular effects (Poursafa and Kelishadi 2010; Frampton et al. 2012; Van Winkle et al. 2015), suggesting a possible link between FFF 3-D printer emissions and cardiovascular events. A previously published study observed that exposure to 3-D printer emissions stimulates acute hypertension and microvascular dysfunction (Stefaniak et al. 2017a).

Surfactant proteins SP-A and SP-D play a critical role in lung host defense by inhibiting inflammation, enhancing the elimination of pathogens and foreign particles, and influencing overall surfactant homeostasis and disease progression (Kingma and Whitsett 2006; Pastva et al. 2007). Recent advances in lung pathogenesis and in understanding the roles of these two pulmonary collectins suggest that SP-A and SP-D may potentially serve as biomarkers of disease or injury (Haczku 2008; Silveyra and Floros 2012; Ley et al. 2014). In our study, we found slightly decreased SP-A (day 8) and SP-D (day 4) levels in BALF. Decreased concentrations of surfactant proteins in BALF were reported as a result of long-term smoking (Honda et al. 1996; Betsuyaku et al. 2004) or as an age-related effect (Hermans et al. 2003; Betsuyaku et al. 2004; Sorensen et al. 2006), perhaps indicating pulmonary damage due to loss of alveolar epithelium integrity.

Lung endothelial and epithelial cells form a functional air-blood barrier that is important for rapid and effective gas exchange between alveoli and microvasculature, and for preventing translocation of micron-size inhaled particles into the circulatory system. However, the nanometer size of particles emitted during additive manufacturing may facilitate penetration of the air-blood barrier, and result in adverse health effects, as shown for polystyrene nanoparticles (Fazlollahi et al. 2013). To further explore the potential systemic toxicity of ABS-emitted particles, we evaluated serum chemistry biomarkers involved in inflammatory and injury processes, as well as biomarkers of muscle, metabolic, liver, and kidney function. Among the 16 markers analyzed, the only significant changes above normal ranges in ABS-treated rats occurred on day 1 of exposure with an increase in creatinine kinase and aspartate aminotransferase, markers of kidney and hepatic function, respectively. A significant increase in other markers of hepatic (day 1) and renal (day 15) damage was noted. However, these changes fell within normal ranges, and returned to air-control levels by day 30 of exposure, indicating a transient systemic toxic effect. Pulmonary findings are consistent with the blood analysis, suggesting that the changes caused by exposure to ABS-emissions, at the durations and dose studied, are minimal and transitory. A similar pattern was observed in a previous study (Zitting and Savolainen 1980), which evaluated the effects of thermo-oxidative degradation products of heated poly(acrylonitrile-butadiene-styrene) at 300–330 °C. Zitting et al. exposed male Wistar rats to a single concentration of degradation products for 1, 3, and 10 days (6 h/night, 5 nights/week), and 3 h post-exposure animals were assessed for adverse effects on lung, liver, kidney, and the brain. The degradation products included styrene (11–24 ppm), carbon monoxide (4–5 ppm), formaldehyde (0.20–0.31 ppm), hydrogen cyanide (0.08–0.67 ppm), acrolein (1.4–1.9 ppm), acrylonitrile (2–4 ppm), and aerosol fraction (8–26 mg/m^3). The authors observed that exposure caused a significant reduction of 7-ethoxycoumarin *O*-deethylation activity (a marker for assessing substrate specificities of cytochrome P450) in lung and kidney, but not in the liver, after one day of exposure. At the same exposure endpoint, a decrease in reduced glutathione concentration (GSH) in the liver and kidney, but not in the lung, was noted, suggesting decreased antioxidant defense. After 3 days of exposure, lung GSH levels remained decreased and returned to control levels by day 10.

At this time, it is unclear if particle number, mass, or surface area is the most relevant metric of toxicity for FFF 3-D printer emissions. Gumperlein et al. (2018) exposed human volunteers to ABS emissions at 1.6×10^6 particles/cm^3 and reported minimal evidence of inflammatory responses based on biomonitoring. Specificlaly, the volunteers' exhaled air showed increased levels of nitric oxide, which might be due to inhaled ultrafine particle-induced eosinophilic inflammation. However, no clinically significant acute changes in the biochemical responses of nasal secretions and urine were found. In an *in vivo* toxicology study, Stefaniak et al. exposed rats once to ABS emissions at 0.9 ± 0.1 mg/m^3 ($D_p \sim 70$ nm) and observed acute hypertension (Stefaniak et al. 2017a). Hence, caution is needed when interpreting the results of the current inhalation study because the lack of significant responses for several toxicological outcomes may not prove the absence of ABS toxicity, but rather be an effect from 1) the choice of exposure metric, and/or 2) the relatively low particle number and mass exposures compared to those employed in other toxicology studies. While the temporal pattern of particulate emissions in the exposure chamber was in the range or higher than observed in real-world settings (McDonnell et al. 2016; Vaisanen et al. 2019), a significant challenge for this and future inhalation toxicology studies of FFF 3-D printer emissions is the generation of consistent daily aerosol exposure with number and mass concentration characteristics that are higher than observed in the real-world workplace to establish a minimal effect and no effect level. Furthermore, careful selection of the most appropriate and relevant

animal species is essential considering the differences in the anatomy of the airways, the characteristics of particle deposition and clearance, which would ultimately have implications in the observed health effects. In addition, a dose-dependence relationship would be relevant to establish some criteria to base the relative safety of FFF 3-D printer emissions.

Conclusions

Repeated whole-body inhalation exposures to FFF 3-D printing emissions (particles at $240 \pm 90\,\mu g/m^3$ concentration, and the listed VOC types at the concentrations reported) released from ABS filament in commercially available desktop 3-D printers for 4 h/day for 1, 4, 8, 15, and 30 days of exposure (4 days/week) caused minimal and transient pulmonary and systemic effects to rats. Our findings suggest that ABS emissions elicited an adaptive response in this exposure paradigm. This adaptive phenomenon refers to when a low stimulating dose of stress is administered that initiates compensatory biological processes (Wiegant et al. 2011). However, considering the significant variability observed in the emission characteristics for one ABS filament and one printer model combination, to multiple printer, filament and operation condition combinations, we cannot exclude the potential of further acute and chronic inflammatory responses, particularly when human case studies report the development of respiratory symptoms and new diagnoses of asthma and allergic rhinitis from workplace 3-D printer exposures (House et al. 2017, Chan et al. 2018).

Disclosure statement

The authors report no conflict of interest.

The findings and conclusions in this report are those of the authors and do not necessarily represent the official position of the National Institute for Occupational Safety and Health, Centers for Disease Control and Prevention. Mention of brand name does not constitute product endorsement.

This work has not been reviewed or approved by and does not necessarily represent the views of, the Commission.

Funding

This investigation was supported by U.S. Consumer Product Safety Commission (CPSC) and the National Institute for Occupational Safety and Health (NIOSH), Project [093909NF].

References

Ahn SH, Lee J, Park SA, Kim WD. 2016. Three-dimensional bio-printing equipment technologies for tissue engineering and regenerative medicine. Tissue Eng Regen Med. 13:663–676.

Anjilvel S, Asgharian B. 1995. A multiple-path model of particle deposition in the rat lung. Fundam Appl Toxicol. 28:41–50.

Arango Duque G, Descoteaux A. 2014. Macrophage cytokines: involvement in immunity and infectious diseases. Front Immunol. 5: 491–491.

Azimi P, Zhao D, Pouzet C, Crain NE, Stephens B. 2016. Emissions of ultrafine particles and volatile organic compounds from commercially available desktop three-dimensional printers with multiple filaments. Environ Sci Technol. 50:1260–1268.

Betsuyaku T, Kuroki Y, Nagai K, Nasuhara Y, Nishimura M. 2004. Effects of ageing and smoking on SP-A and SP-D levels in bronchoalveolar lavage fluid. Eur Respir J. 24:964–970.

Castranova V, Robinson VA, Tucker JH, Schwegler D, Rose DA, DeLong DS, Frazer DG. 1987. Time course of pulmonary response to inhalation of cotton dust in guinea pigs and rats. Cotton dust: proceedings of Eleventh Cotton Dust Research Conference, Beltwide Cotton Research Conferences; Dallas, Texas.

Chan FL, House R, Kudla I, Lipszyc JC, Rajaram N, Tarlo SM. 2018. Health survey of employees regularly using 3D printers. Occup Med (Lond). 68:211–214.

Davis AY, Zhang Q, Wong JPS, Weber RJ, Black MS. 2019. Characterization of volatile organic compound emissions from consumer level material extrusion 3D printers. Build Environ. 160: 106209.

Deng Y, Cao SJ, Chen A, Guo Y. 2016. The impact of manufacturing parameters on submicron particle emissions from a desktop 3D printer in the perspective of emission reduction. Build Environ. 104: 311–319.

Ding S, Ng BF, Shang X, Liu H, Lu X, Wan MP. 2019. The characteristics and formation mechanisms of emissions from thermal decomposition of 3D printer polymer filaments. Sci Total Environ. 692: 984–994.

Farcas MT, Stefaniak AB, Knepp AK, Bowers L, Mandler WK, Kashon M, Jackson SR, Stueckle TA, Sisler JD, Friend SA, et al. 2019. Acrylonitrile butadiene styrene (ABS) and polycarbonate (PC) filaments three-dimensional (3-D) printer emissions-induced cell toxicity. Toxicol Lett. 317:1–12.

Fazlollahi F, Kim YH, Sipos A, Hamm-Alvarez SF, Borok Z, Kim KJ, Crandall ED. 2013. Nanoparticle translocation across mouse alveolar epithelial cell monolayers: species-specific mechanisms. Nanomedicine. 9:786–794.

Frampton MW, Bausch J, Chalupa D, Hopke PK, Little EL, Oakes D, Stewart JC, Utell MJ. 2012. Effects of outdoor air pollutants on platelet activation in people with type 2 diabetes. Inhal Toxicol. 24: 831–838.

Fujii T, Hayashi S, Hogg JC, Mukae H, Suwa T, Goto Y, Vincent R, van Eeden SF. 2002. Interaction of alveolar macrophages and airway epithelial cells following exposure to particulate matter produces mediators that stimulate the bone marrow. Am J Respir Cell Mol Biol. 27:34–41.

Goto Y, Ishii H, Hogg JC, Shih CH, Yatera K, Vincent R, van Eeden SF. 2004. Particulate matter air pollution stimulates monocyte release from the bone marrow. Am J Respir Crit Care Med. 170: 891–897.

Gu J, Wensing M, Uhde E, Salthammer T. 2019. Characterization of particulate and gaseous pollutants emitted during operation of a desktop 3D printer. Environ Int. 123:476–485.

Gumperlein I, Fischer E, Dietrich-Gumperlein G, Karrasch S, Nowak D, Jorres RA, Schierl R. 2018. Acute health effects of desktop 3D printing (fused deposition modeling) using acrylonitrile butadiene styrene and polylactic acid materials: an experimental exposure study in human volunteers. Indoor Air. 28:611–623.

Haczku A. 2008. Protective role of the lung collectins surfactant protein A and surfactant protein D in airway inflammation. J Allergy Clin Immunol. 122:861–879.

Hermans C, Dong P, Robin M, Jadoul M, Bernard A, Bersten AD, Doyle IR. 2003. Determinants of serum levels of surfactant proteins A and B and Clara cell protein CC16. Biomarkers. 8:461–471.

Honda Y, Takahashi H, Kuroki Y, Akino T, Abe S. 1996. Decreased contents of surfactant proteins A and D in BAL fluids of healthy smokers. Chest. 109:1006–1009.

House R, Rajaram N, Tarlo SM. 2017. Case report of asthma associated with 3D printing. Occup Med (Lond). 67:652–654.

Kim Y, Yoon C, Ham S, Park J, Kim S, Kwon O, Tsai PJ. 2015. Emissions of nanoparticles and gaseous material from 3D printer operation. Environ Sci Technol. 49:12044–12053.

Kingma PS, Whitsett JA. 2006. In defense of the lung: surfactant protein A and surfactant protein D. Curr Opin Pharmacol. 6:277–283.

Koh TJ, DiPietro LA. 2011. Inflammation and wound healing: the role of the macrophage. Expert Rev Mol Med. 13:e23.

Ley B, Brown KK, Collard HR. 2014. Molecular biomarkers in idiopathic pulmonary fibrosis. Am J Physiol Lung Cell Mol Physiol. 307:L681–L691.

Lorenz HP, Longaker MT. 2008. Chapter 191–208, Wounds: biology, pathology, and management. In: NJAe, editor. Surgery. New York (NY): Springer.

Mandler WK, Qi C, Orandle MS, Sarkisian K, Mercer RR, Stefaniak AB, Knepp AK, Bowers LN, Battelli LA, Shaffer J, et al. 2019. Mouse pulmonary response to dust from sawing Corian®, a solid-surface composite material. J Toxicol Environ Health Part A. 82: 645–663.

McDonnell B, Guzman XJ, Dolack M, Simpson TW, Cimbala JM. 3D Printing in the Wild: A Preliminary Investigation of Air Quality in College Maker Spaces. Solid Freeform Fabrication Symposium Proceedings. 2016.

Mosser DM. 2003. The many faces of macrophage activation. J Leukoc Biol. 73:209–212.

Nielsen GD, Alarie Y. 1982. Sensory irritation, pulmonary irritation, and respiratory stimulation by airborne benzene and alkylbenzenes: Prediction of safe industrial exposure levels and correlation with their thermodynamic properties. Toxicol Appl Pharmacol. 65: 459–477.

Nurkiewicz TR, Porter DW, Barger M, Castranova V, Boegehold MA. 2004. Particulate matter exposure impairs systemic microvascular endothelium-dependent dilation. Environ Health Perspect. 112: 1299–1306.

Nurkiewicz TR, Porter DW, Hubbs AF, Cumpston JL, Chen BT, Frazer DG, Castranova V. 2008. Nanoparticle inhalation augments particle-dependent systemic microvascular dysfunction. Part Fibre Toxicol. 5:1.

Oberdorster G, Oberdorster E, Oberdorster J. 2005. Nanotoxicology: an emerging discipline evolving from studies of ultrafine particles. Environ Health Perspect. 113:823–839.

Pastva AM, Wright JR, Williams KL. 2007. Immunomodulatory roles of surfactant proteins A and D: implications in lung disease. Proc Am Thorac Soc. 4:252–257.

Potter PM, Al-Abed SR, Lay D, Lomnicki SM. 2019. VOC emissions and formation mechanisms from carbon nanotube composites during 3D printing. Environ Sci Technol. 53:4364–4370.

Poursafa P, Kelishadi R. 2010. Air pollution, platelet activation and atherosclerosis. Inflamm Allergy Drug Targets. 9:387–392.

Rundell KW, Hoffman JR, Caviston R, Bulbulian R, Hollenbach AM. 2007. Inhalation of ultrafine and fine particulate matter disrupts systemic vascular function. Inhal Toxicol. 19:133–140.

Silveyra P, Floros J. 2012. Genetic variant associations of human SP-A and SP-D with acute and chronic lung injury. Front Biosci (Landmark Ed). 17:407–429.

Simon TR, Lee WJ, Spurgeon BE, Boor BE, Zhao F. 2018. An experimental study on the energy consumption and emission profile of fused deposition modeling process. Procedia Manuf. 26:920–928.

Sittig M. 1985. Handbook of toxic and hazardous chemicals and carcinogens. 2nd ed. Park Ridge (NJ): Noyes Publications.

Sorensen GL, Hjelmborg J, Kyvik KO, Fenger M, Hoj A, Bendixen C, Sorensen TI, Holmskov U. 2006. Genetic and environmental influences of surfactant protein D serum levels. Am J Physiol Lung Cell Mol Physiol. 290:L1010–L1017.

Stefaniak A, Johnson A, Du Preez S, Hammond D, Wells J, Ham J, LeBouf R, Martin S, Duling M, Bowers L, et al. 2019. Insights into emissions and exposures from use of industrial-scale additive manufacturing machines. Saf Health Work. 10:229–236.

Stefaniak A, LeBouf R, Duling M, Yi J, Abukabda A, McBride C, Nurkiewicz T. 2017a. Inhalation exposure to three-dimensional printer emissions stimulates acute hypertension and microvascular dysfunction. Toxicol Appl Pharmacol. 335:1–5.

Stefaniak A, LeBouf R, Yi J, Ham J, Nurkewicz T, Schwegler-Berry D, Chen B, Wells J, Duling M, Lawrence R, et al. 2017b. Characterization of chemical contaminants generated by a desktop fused deposition modeling 3-dimensional Printer. J Occup Environ Hyg. 14:540–550.

Stephens B, Azimi P, El Orch Z, Ramos T. 2013. Ultrafine particle emissions from desktop 3D printers. Atmos Environ. 79:334–339.

Trenfield SJ, Awad A, Madla CM, Hatton GB, Firth J, Goyanes A, Gaisford S, Basit AW. 2019. Shaping the future: recent advances of 3D printing in drug delivery and healthcare. Expert Opin Drug Deliv. 16:1081–1094.

U.S. Environmental Protection Agency. 1987. Health assessment document for acetaldehyde. Research Triangle Park (NC): Environmental Criteria and Assessment Office, Office of Health and Environmental Assessment, Office of Research and Development. EPA/600/8-86-015A.

Vaisanen AJK, Hyttinen M, Ylonen S, Alonen L. 2019. Occupational exposure to gaseous and particulate contaminants originating from additive manufacturing of liquid, powdered, and filament plastic materials and related post-processes. J Occup Environ Hyg. 16: 258–271.

Van Winkle LS, Bein K, Anderson D, Pinkerton KE, Tablin F, Wilson D, Wexler AS. 2015. Biological dose response to PM2.5: effect of particle extraction method on platelet and lung responses. Toxicol Sci. 143:349–359.

Wang J, Yu Y, Guo J, Lu W, Wei Q, Zhao Y. 2020. The construction and application of three-dimensional biomaterials. Adv Biosyst. 4: e1900238.

Wiegant FA, Prins HA, Van Wijk R. 2011. Postconditioning hormesis put in perspective: an overview of experimental and clinical studies. Dose Response. 9:209–224.

Wojtyła S, Klama P, Baran T. 2017. Is 3D printing safe? Analysis of the thermal treatment of thermoplastics: ABS, PLA, PET, and nylon. J Occup Environ Hyg. 14:D80–D85.

Wojtyła S, Śpiewak K, Baran T. 2020. Synthesis, characterization and activity of doped graphitic carbon nitride materials towards photocatalytic oxidation of volatile organic pollutants emitted from 3D printer. J Photochem Photobiol A. 391:112355.

Yi J, Duling MG, Bowers LN, Knepp AK, LeBouf RF, Nurkiewicz TR, Ranpara A, Luxton T, Martin SB, Burns DA, et al. 2019. Particle and organic vapor emissions from children's 3-D pen and 3-D printer toys. Inhalation Toxicol. 31:432–445.

Young JT. 1981. Histopathologic examination of the rat nasal cavity. Fundam Appl Toxicol. 1:309–312.

Zhang Q, Pardo M, Rudich Y, Kaplan-Ashiri I, Wong JP, Davis A, Black M, Weber R. 2019. Chemical composition and toxicity of particles emitted from a consumer-level 3D printer using various materials. Environ Sci Technol. 53:12054–12061.

Zhang Q, Wong J, Davis A, Black M, Weber R. 2017. Characterization of particle emissions from consumer fused deposition modeling 3D printers. Aerosol Sci Technol. 51:1275–1286.

Zitting A, Savolainen H. 1980. Effects of single and repeated exposures to thermo-oxidative degradation products of poly(acrylonitrile-butadiene-styrene) (ABS) on rat lung, liver, kidney, and brain. Arch Toxicol. 46:295–304.